Simulation of dissolution and precipitation in porous media

Qinjun Kang[1]

Los Alamos National Laboratory, Los Alamos, New Mexico, USA

Dongxiao Zhang

Los Alamos National Laboratory, Los Alamos, New Mexico, USA

Shiyi Chen[2]

Department of Mechanical Engineering, Johns Hopkins University, Baltimore, Maryland, USA

[1]   We apply the lattice-Boltzmann method to simulate fluid flow and dissolution and precipitation in the reactive solid phase in a porous medium. Both convection and diffusion as well as temporal geometrical changes in the pore space are taken into account. The numerical results show that at high Peclet and Peclet-Damkohler numbers, a wormhole is formed and permeability increases greatly because of the dissolution process. At low Peclet and high Peclet-Damkohler numbers, reactions mainly occur at the inlet boundary, resulting in the face dissolution and the slowest increase of the permeability in the dissolution process. At moderate Peclet and Peclet-Damkohler numbers, reactions are generally nonuniform, with more in the upstream and less in the downstream. At very small Peclet-Damkohler number, dissolution or precipitation is highly uniform, and these two processes can be approximately reversed by each other. These numerical examples have not been yet confirmed by physical experimentation. Nevertheless, we believe that these simulation results can serve to estimate the effects of dissolution and precipitation during reactive fluid flow.   *INDEX TERMS:* 1815 Hydrology: Erosion and sedimentation; 5104 Physical Properties of Rocks: Fracture and flow; 5114 Physical Properties of Rocks: Permeability and porosity; *KEYWORDS:* dissolution/precipitation, Peclet number, Damkohler number, porous media, lattice-Boltzmann method

1. Introduction

[2]   The coupled transport and reaction of fluids in porous media or fractures plays a crucial role in a variety of scientific, industrial, and engineering processes, such as stimulation of petroleum reservoirs, environmental contaminant transport, mineral mining, geologic sequestration of carbon dioxide, chemical weathering, diagenesis, concrete degradation, bioremediation, and dissolution/formation of hydrates.

[3]   These applications typically involve multiple processes such as convection, diffusion, and reaction. Complicating matters even more is the evolution of porous media that results from dissolution/precipitation. Such evolution may significantly and continuously modify the hydrologic properties of the media. Changes in hydrologic properties (e.g., porosity, fracture aperture, and tortuosity) result in changes in permeability and effective mass diffusivity. Therefore such changes are coupled with subsequent fluid flow, solute transport, and surface reactions.

[4]   Because of its importance, this problem has been studied by various approaches: From semianalytical investigations [*Dijk and Berkowitz*, 1998], to experimental studies [*Daccord*, 1987], to numerical simulations [*Salles et al.*, 1993]; from solving macroscopic partial differential equations [*Chadam et al.*, 1986; *Ortoleva et al.*, 1987; *Chen and Ortoleva*, 1990; *Steefel and Lasaga*, 1990, 1994; *Aharonov et al.*, 1995, 1997; *Liu et al.*, 1997; *Ormond and Ortoleva*, 2000], to microscopic studies [*Daccord*, 1987; *Wells et al.*, 1991; *Janecky et al.*, 1992; *Kelemen et al.*, 1995; *Salles et al.*, 1993; *Bekri et al.*, 1995, 1997; *Dijk and Berkowitz*, 1998], to analog network simulations [*Hoefner and Fogler*, 1988; *Fredd and Fogler*, 1998].

[5]   At a Darcy scale and under the condition that the dissolution process does not increase the porosity dramatically, fingering, the formation of channels wherein the dissolution is not complete, has been modeled using the

---

[1]Also at Department of Mechanical Engineering, Johns Hopkins University, Baltimore, Maryland, USA.

[2]Also at Center for Computational Science and Engineering and Laboratory for Turbulence and Complex System, Peking University, Beijing, China.

Darcy equation in both homogeneous and heterogeneous porous media [*Chen and Ortoleva*, 1990; *Steefel and Lasaga*, 1990]. Wormholing, the formation of channels wherein the matrix is completely removed through dissolution, has been achieved numerically using Brinkman's equation [*Liu et al.*, 1997; *Ormond and Ortoleva*, 2000].

[6] At a microscopic scale, in an experiment performed on plaster, *Daccord* [1987] observed the formation of a highly branched wormhole network. *Wells et al.* [1991] used a lattice-gas automata (LGA) to simulate the coupled solute transport and chemical reaction at mineral surfaces and in pore networks. *Janecky et al.* [1992] applied a similar method for simulating geochemical systems.

[7] Using a combination of an experimental study and lattice-Boltzmann (LB) simulations, *Kelemen et al.* [1995] demonstrated the phenomenon of channel growth with and without an initial solution front. *Salles et al.* [1993] used numerical schemes partly based on random walks to study deposition in porous media in the quasi-steady limit where the geometrical changes are very slow.

[8] *Bekri et al.* [1995] applied similar numerical schemes in a study that focused on the dissolution of porous media. When simulating dissolution in the Menger sponge, they found that dissolution is expected to occur as follows: For small Peclet-Damkohler (*PeDa*) and small Peclet (*Pe*) numbers, dissolution occurs over all the solid walls. For large *PeDa* and large *Pe*, dissolution occurs along the main channel parallel to the flow direction. For *Pe* and *PeDa* of order one, dissolution occurs isotropically around the central cavity and symmetrically along the flow direction. For large *PeDa* and small *Pe*, dissolution occurs around the central cavity and then along the main channels. Under the same conditions, *Bekri et al.* [1997] used a finite difference scheme to study the deposition and/or dissolution of a single solute in a single fracture.

[9] *Dijk and Berkowitz* [1998] developed a semianalytical model of precipitation and dissolution by the first-order reactions in two-dimensional fractures. They took into account the change in fracture shape. They also proposed applications to realistic geochemical conditions. Their results are as follows: Precipitation in the fracture is highly uniform for (1) low *PeDa* and typical *Pe* and (2) typical *PeDa* and high *Pe*. Precipitation in the fracture is generally nonuniform for typical *PeDa* and typical *Pe*. Precipitation in the fracture is highly nonuniform for (1) high *PeDa* and typical *Pe* and (2) typical *PeDa* and low *Pe*.

[10] The dissolution phenomenon also has been investigated using analog network simulations [*Hoefner and Fogler*, 1988; *Fredd and Fogler*, 1998]. The simulation results were similar (qualitatively) to results obtained from acidizing experiments.

[11] In previous work [*Kang et al.*, 2002], we developed an LB model [*Chen and Doolen*, 1998] to simulate coupled flow and chemical reaction in porous media. We took a systematic approach in considering the dynamic processes of convection, diffusion, and reaction, as well as the complex geometry of natural porous media and its evolution (the latter caused by chemical reaction). The simulation results agreed qualitatively with the experimental and theoretical analyses conducted by other researchers. Furthermore, our results substantiated the previous finding that there exists an optimal injection rate at which (1) the wormhole is formed

and (2) the number of pore volumes of the injected fluid to break through is minimized. The results also confirmed the following experimentally observed phenomenon: as HCl changes to HAc, the optimal injection rate decreases and the corresponding minimized number of pore volumes to break through increases.

[12] In this study, we extend the LB method so that we can investigate the coupled dissolution and precipitation process in a simplified porous medium. Our objective is to study the effects of some important dimensionless control parameters, such as the *Pe* and *PeDa* numbers. We also examine the conditions necessary for approximately reversing dissolution and precipitation.

2. Model and Theory

2.1. Lattice-Boltzmann Method for Fluid Flow

[13] The following LB equation can simulate fluid flow:

$$f_i(\mathbf{x} + \mathbf{e}_i \delta_t, t + \delta_t) = f_i(\mathbf{x}, t) - \frac{f_i(\mathbf{x}, t) - f_i^{eq}(\rho, \mathbf{u}, T)}{\tau}, \quad (1)$$

where f_i is the particle velocity distribution function along the i direction, δ_t is the time increment, τ is the relaxation time related to the kinematic viscosity by $\nu = (\tau - 0.5)RT$, and f_i^{eq} is the corresponding equilibrium distribution function. This function has the following form:

$$f_i^{eq}(\rho, \mathbf{u}, T) = \omega_i \rho \left[1 + \frac{\mathbf{e}_i \cdot \mathbf{u}}{RT} + \frac{(\mathbf{e}_i \cdot \mathbf{u})^2}{2(RT)^2} - \frac{\mathbf{u}^2}{2RT} \right], \quad (2)$$

where R is the gas constant; ρ, $\mathbf{u}$, and T are the density, velocity, and temperature of the fluid, respectively; $\mathbf{e}_i$ are the discrete velocities; and ω_i are the associated weight coefficients. Figure 1 shows a commonly used two-dimensional, nine-speed LB model, for which we have $RT = 1/3$ and

$$\mathbf{e}_i = \begin{cases} 0 & i = 0, \\ \left(\cos \frac{(i-1)\pi}{2}, \sin \frac{(i-1)\pi}{2} \right) & i = 1 - 4, \quad (3) \\ \sqrt{2} \left(\cos \left[\frac{(i-5)\pi}{2} + \frac{\pi}{4} \right], \sin \left[\frac{(i-5)\pi}{2} + \frac{\pi}{4} \right] \right) & i = 5 - 8. \end{cases}$$
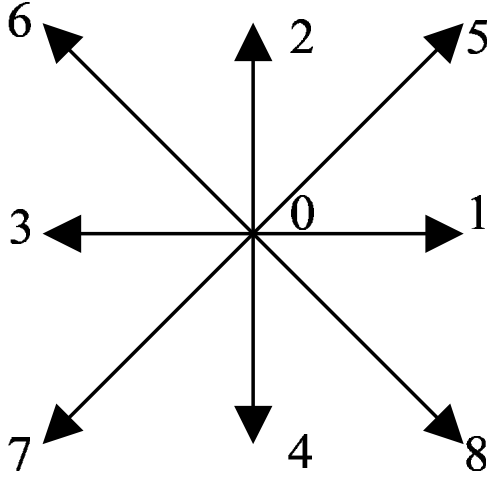
The corresponding weight coefficients are $\omega_0 = 4/9$, $\omega_i = 1/9$ for $i = 1, 2, 3, 4$, and $\omega_i = 1/36$ for $i = 5, 6, 7, 8$. The fluid's density and velocity are calculated using

$$\rho = \sum_i f_i, \quad (4)$$

$$\rho \mathbf{u} = \sum_i \mathbf{e}_i f_i. \quad (5)$$

[14] Using the Chapman-Enskog expansion, we can prove that the LB equation (1) recovers the correct continuity and momentum equations at the Navier-Stokes level [*Qian et al*, 1992; *Chen et al*, 1992]:

$$\frac{\partial \rho}{\partial t} + \nabla \cdot (\rho \mathbf{u}) = 0, \quad (6)$$

Figure 1. Schematic illustration of the two-dimensional, nine-speed lattices.

$$\frac{\partial(\rho\mathbf{u})}{\partial t} + \nabla \cdot (\rho\mathbf{uu}) = -\nabla p + \nabla \cdot [\rho\nu(\nabla\mathbf{u} + \mathbf{u}\nabla)], \quad (7)$$

where $p = \rho\{R\}T$ is the fluid pressure.

2.2. Lattice-Boltzmann Method for Solute Transport

[15] In this study, we assume that the solute concentration is sufficiently low so that we can describe the solute transport using another distribution function, g_i, which satisfies a similar evolution equation as f_i:

$$g_i(\mathbf{x} + \mathbf{e}_i\delta_t, t + \delta_t) = g_i(\mathbf{x}, t) - \frac{g_i(\mathbf{x}, t) - g_i^{eq}(C, \mathbf{u}, T)}{\tau_s}, \quad (8)$$

where τ_s is the relaxation time related to the diffusivity by $D = (\tau_s - 0.5)RT$ and g_i^{eq} is the corresponding equilibrium distribution function. This latter function has the following form:

$$g_i^{eq}(C, \mathbf{u}, T) = \omega_i C\left[1 + \frac{\mathbf{e}_i \cdot \mathbf{u}}{RT} + \frac{(\mathbf{e}_i \cdot \mathbf{u})^2}{2(RT)^2} - \frac{\mathbf{u}^2}{2RT}\right], \quad (9)$$

where C is the solute concentration. This concentration is defined by

$$C = \sum_i g_i. \quad (10)$$

Using the Chapman-Enskog expansion technique, we can prove that the LB equation (8) recovers the following convection-diffusion equation [*Dawson et al.*, 1993]:

$$\frac{\partial C}{\partial t} + (\mathbf{u} \cdot \nabla)C = \nabla \cdot (D\nabla C). \quad (11)$$

2.3. Boundary Conditions

[16] In this study, we assume the rate of deformation for the solid surface to be so slow that we can determine the velocity field in the fluid at any time by solving the evolution equation of the particle distribution function with

a bounce back condition at the walls. Macroscopically, this corresponds to the quasi-static hypothesis that the velocity field is determined by Navier-Stokes equation with no-slip condition at the current position of walls. The bounce back LB boundary condition at the wall nodes requires little computational time. Even though it has only first-order accuracy at the boundaries, this technique remains the most practical way to handle the no-slip condition in complex geometries, such as those encountered in real porous media [*Chen and Doolen*, 1998].

[17] We consider the first-order kinetic reaction model at the solid-fluid interface:

$$D\frac{\partial C}{\partial n} = k_r(C - C_s), \quad (12)$$

where D is the diffusivity, C is the solute concentration at the interface, C_s is the saturated concentration, k_r is the local reaction rate constant, and n is the direction normal to the interface pointing toward the fluid phase.

[18] Equation (12) describes a boundary condition for a macroscopic level surface reaction. *Kang et al.* [2002] formulated a boundary condition for the distribution function. We have based our approach on the observation that at a stationary wall, the nonequilibrium portion of the distribution function is proportional to the dot product of the function's microscopic velocity and the concentration gradient. For example, if we take a wall node in the left bottom corner (see Figure 2), we can determine g_3, g_4, and g_7 based on the streaming process of the particle distribution function g_i. In contrast, we must determine g_1, g_2, g_5, g_6, and g_8 using the boundary conditions. To determine the solute concentration at this node, we use the known distribution function g_7 [*Kang et al.*, 2002]:

$$C = \frac{g_7 + \beta C_s}{\beta + \omega_7}, \quad (13)$$

where $\beta = \frac{1}{32}(k_r/D)$. On the basis of C and $\mathbf{u}$, we can calculate g_i^{eq} from equation (9). From this result we then can calculate the unknown distribution functions:

$$g_1 = g_1^{eq} + g_3^{eq} - g_3, \quad (14)$$
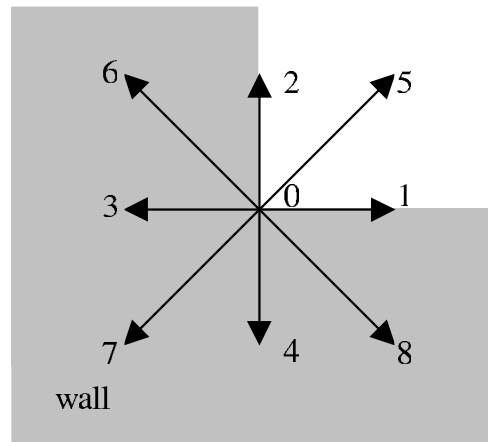
Figure 2. A wall node at the left bottom corner.

$$g_2 = g_2^{eq} + g_4^{eq} - g_4, \qquad (15)$$

$$g_5 = g_5^{eq} + g_7^{eq} - g_7, \qquad (16)$$

$$g_6 = g_6^{eq} + \frac{g_3 - g_4}{4\sqrt{2}}, \qquad (17)$$

$$g_8 = g_8^{eq} - \frac{g_3 - g_4}{4\sqrt{2}}. \qquad (18)$$

2.4. Dimensionless Control Parameters

[19] Simple dimensional analysis suggests that three dimensionless parameters control this process. They are the relative concentration $\psi = C_0/C_s$, Peclet number $Pe = UL/D$, and Damkohler number $Da = k_r/U$. In the definition of these parameters, C_0 is the concentration of the inflowing solution, and U and L are characteristic velocity and length of the system, respectively.

[20] The Peclet number describes the effect of advection relative to that of molecular diffusion on the solute transport. The Damkohler number describes the effect of reaction relative to that of convection. Their product $PeDa = k_rL/D$, describes the reaction's effect relative to diffusion. This product is frequently used because the convection diminishes at the interface. Our focus during this study is on how Pe and $PeDa$ affect the dissolution/precipitation process.

3. Simulation Results and Discussion

[21] Figure 3 shows the two-dimensional geometry used in our simulations, as well as the initial distribution of the solute concentration. The initial medium is 100 by 195 (in lattice units), with a few arrays of void space at the left and right boundaries. In this medium are two horizontal fractures with widths of 30 and 4, respectively. For the smaller fracture, the Knudsen number is not very small; as a result, the fluid flow in it cannot be treated as a continuum flow. Instead, there will be a mean slip velocity on wall boundary because of the kinetic nature of the LB method [*Nie et al.*, 2002]. As dissolution helps the channel grow larger, more grids are used, and as a result the flow can be treated as a continuum flow. The density (pressure) is fixed at both the left inlet and the right outlet boundaries [*Zou and He*, 1997].

[22] Initially, the solution is saturated and no surface reaction occurs. When flow achieves a steady state, the inflowing fluid changes into a pure solvent. It is then that dissolution occurs. After part of the medium dissolves, the inflowing fluid changes to a supersaturated solution whose solute concentration is twice that of a saturated solution. Precipitation takes place soon after.

[23] To make sure that steady state is achieved at the current geometry, we perform the flow simulation every time there is a change in pore or grain nodes. Because dissolution or precipitation occurs only at the solid-liquid interface, each change does not incur a dramatic change in porosity.

[24] We used the following four combinations of Pe and $PeDa$ values to investigate how such combinations affect the dissolution/precipitation process: (1) large Pe and $PeDa$
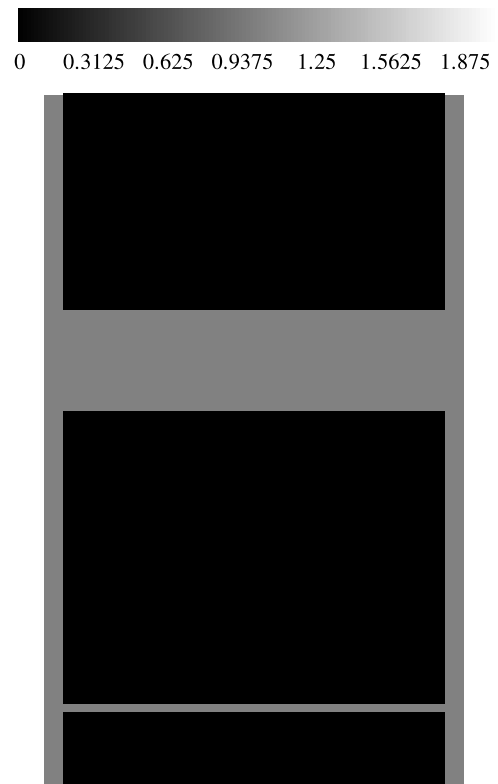
0	0.3125	0.625	0.9375	1.25	1.5625	1.875

Figure 3. Schematic illustration of the two-dimensional geometry and the initial distribution of the solute concentration. See color version of this figure at back of this issue.

($Pe = 45$, $PeDa = 7.5$), (2) moderate Pe and $PeDa$ ($Pe = 0.45$, $PeDa = 0.075$), (3) small Pe and $PeDa$ ($Pe = 0.0045$, $PeDa = 0.00075$), and (4) small Pe but large $PeDa$ ($Pe = 0.0045$, $PeDa = 7.5$).

[25] The characteristic length in the definition of Pe and $PeDa$ is the width of the larger fracture of the original medium. The characteristic velocity is the center line velocity of the fracture at its initial steady state. The actual values of Pe and $PeDa$ change with time as a result of dissolution and/or precipitation.

[26] Figure 4 shows the resultant geometry and distribution of solute concentration (caused by dissolution) just before the inflowing liquid changes from pure solvent to supersaturated solution. The black regions indicate solids. Figure 4a shows the dissolution process as diffusion-limited. In this case, the highest dissolution rates occur on the walls that face the inlet boundary and on the walls of the larger fracture. These rates are high because the flow rapidly renews the solution in these regions.

[27] However, the smaller fracture remains intact, except for the upstream region. Because the fluid flows very slowly in this fracture, the diffusion does not transport much solute out of the fracture during such a short time frame. As a result, the solute concentration in the small fracture is always close to the saturated one, thereby making the dissolution rate very low. Because the larger fracture dissolves faster than the smaller one, the dissolution process is unstable when both Pe and $PeDa$ are large. In addition, this case also gives rise to the "wormholing" phenomenon, in
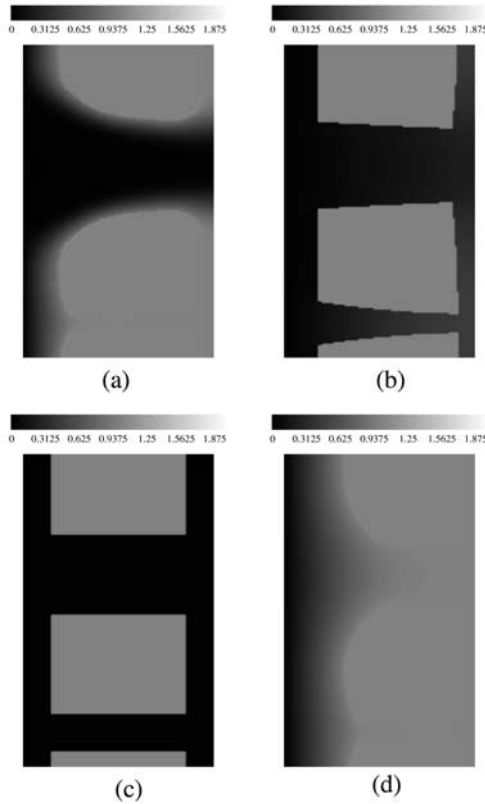
Figure 4. Resulting geometry and distribution of the solute concentration due to dissolution, just before the inflowing fluid is switched from pure solvent to super-saturated solution. The concentration is normalized by the saturated one: (a) $Pe = 45$, $PeDa = 7.5$; (b) $Pe = 0.45$, $PeDa = 0.075$; (c) $Pe = 0.0045$, $PeDa = 0.00075$; (d) $Pe = 0.0045$, $PeDa = 7.5$. See color version of this figure at back of this issue.

which the initially large fractures dominate at the end of the dissolution process. Our observations agree with those of *Bekri et al.* [1995].

[28] In Figure 4b, both Pe and $PeDa$ are moderate. Dissolution occurs on the walls facing the inlet boundary, as well as on the walls of both fractures. Whereas the upstream walls dissolve uniformly, the fracture walls do so nonuniformly. As pure solvent penetrates the fractures, the fracture walls dissolve and the dissolution increases the solute's concentration. As a result, the dissolution slows down along the direction of the flow.

[29] Figure 4b also shows that the low-concentration solution penetrates the larger fracture more quickly than the smaller fracture (the solution is downstream in the larger fracture but only midstream in the smaller fracture). The reason for this difference in speed is that the actual Da is smaller for the larger fracture than for the smaller fracture.

[30] When both Pe and $PeDa$ are small, the dissolution process is reaction-limited. The dissolution rate is low enough for the solution's concentration field to remain nearly uniform all the time. Therefore we expect the dissolution to be uniform over all the solid walls, as shown in Figure 4c.

[31] When Pe is small but $PeDa$ is large, dissolution occurs mostly on the walls that face the inlet flow boundary

and are on the very upstream part of the fracture. As shown in Figure 4d, the original fractures do not expand and no dissolution takes place downstream. This is the face dissolution, where solids are dissolved starting from the inlet flow face and the permeability increase is not significant because no dominant channels are formed, as mentioned in the paper by *Kang et al.* [2002]. In contrast to case c, the solute concentration distribution is highly nonuniform as it increases along the fracture direction.

[32] Figure 5 shows the resultant geometry and distribution of solute concentration (due to precipitation) when one of the fractures is clogged sometime after the inflowing fluid changes from pure solvent to supersaturated solution. Combining Figure 5 with Figure 4 reveals four different precipitation patterns among the four cases. In case a, precipitation occurs mostly on the larger fracture walls, particularly in the wider upstream part. As a result, permeability decreases rapidly, as shown in Figure 6a.

[33] Figures 4b and 5b show that for case b precipitation occurs on the walls of both fractures, as well as on the walls that face the inlet boundary. Much like the dissolution process described earlier, precipitation also slows down along the flow direction. The smaller fracture clogs first.

[34] Case c mirrors the reversed process of dissolution in that precipitation is uniform over all the solid walls, as
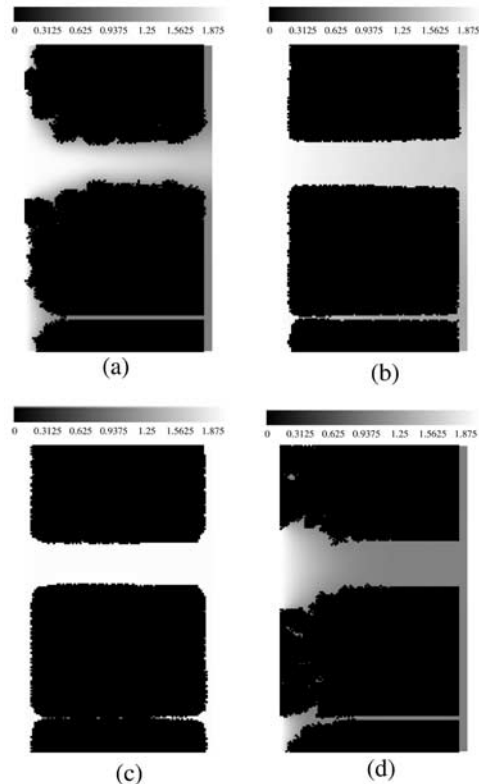
Figure 5. Resulting geometry and distribution of the solute concentration due to precipitation, when a fracture is clogged. The concentration is normalized by the saturated one: (a) $Pe = 45$, $PeDa = 7.5$; (b) $Pe = 0.45$, $PeDa = 0.075$; (c) $Pe = 0.0045$, $PeDa = 0.00075$; (d) $Pe = 0.0045$, $PeDa = 7.5$. See color version of this figure at back of this issue.
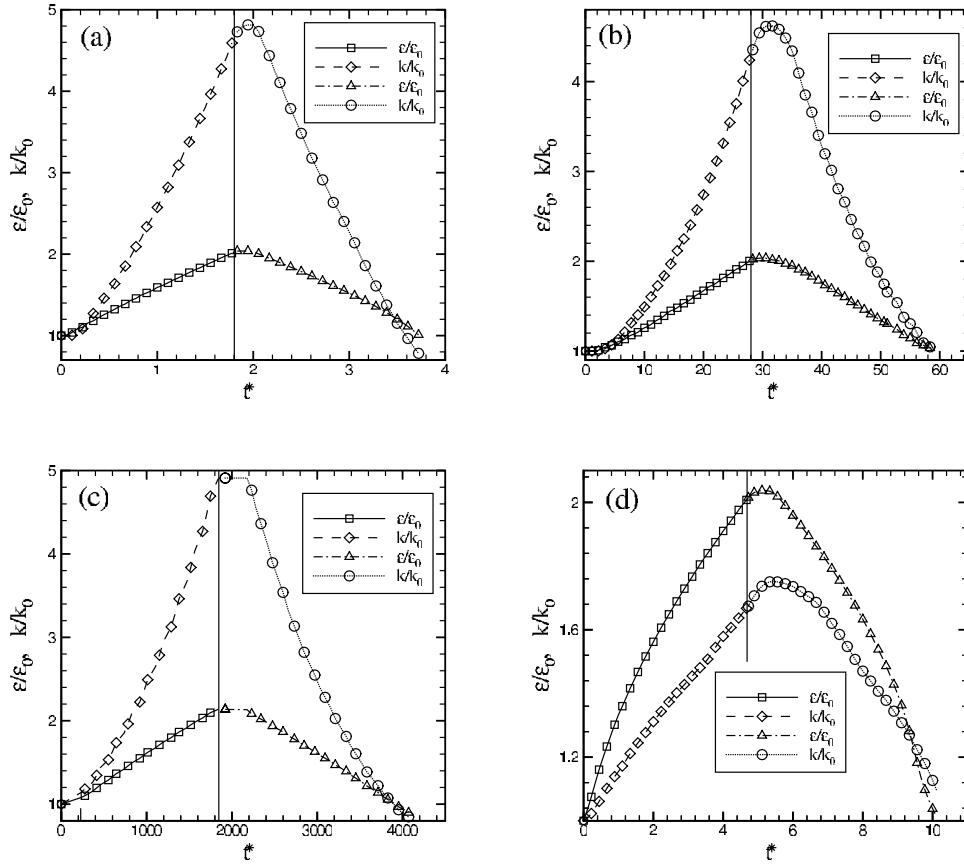
Figure 6. Time evolution of normalized porosity and permeability. k_0, ϵ_0 are permeability and porosity of the initial geometry, respectively. Time is normalized by characteristic time L^2/D. The vertical lines indicate the start of precipitation: (a) $Pe = 45$, $PeDa = 7.5$; (b) $Pe = 0.45$, $PeDa = 0.075$; (c) $Pe = 0.0045$, $PeDa = 0.00075$; (d) $Pe = 0.0045$, $PeDa = 7.5$.

shown in Figures 4c and 5c. As a result, the smaller fracture clogs first. The solute concentration is uniform.

[35] In case d, precipitation occurs mostly on the walls facing the inlet boundary. However, some precipitation does occur in the small fracture, and as a result the small fracture clogs, as shown in Figures 4d and 5d. Because the solute has a high reaction rate but low convection and diffusion, it is quickly consumed at the upstream. Moreover, the concentration remains almost completely saturated in most of the pore spaces, as shown in Figure 5d.

[36] Figure 6 shows the time evolution of normalized porosity and permeability, whereas Figure 7 shows the normalized permeability-porosity relationship. The vertical lines in Figure 6 mark the beginning of precipitation. As shown in Figure 6, the reaction goes faster in cases a and d; in both cases, $PeDa$ is large. In case c, $PeDa$ is small, and as a result the reaction rate is the slowest of the four.

[37] Table 1 lists normalized permeability values for different dissolution cases that have a normalized porosity value of 2. As shown in this table, the permeability value increases most in case a, where a dominant wormhole forms. The value increases the least in case d, where face dissolution dominates [Kang et al., 2002].

[38] Except for case c, permeability and porosity values continue to increase after the inflowing fluid changes to a supersaturated solution. The principal reason for such a

sustained increase is that the pore spaces are filled with low-concentration solution. This solution continues to dissolve the solids before it is replaced with a more concentrated solution by convection and diffusion.

[39] We also found that the maximum value of permeability lags behind that of porosity. In other words, there is a short period of time when porosity decreases while permeability increases. This phenomenon is most salient in case b. In addition to other reasons, the geometry plays an important role. As shown in Figure 4b, both fractures are constricted. Precipitation on the wider, upstream part of the fractures and dissolution on the narrower, downstream part help the fracture walls become parallel to the horizontal direction. Thus permeability increases even though more solids are precipitated than dissolved. In case c, the reaction is so slow that the dilute solution in the system is replaced by a more concentrated one before the former can dissolve any of the solids.

[40] The same conclusions can be drawn from Figure 7. Additionally, in case c, the permeability-porosity relationship curve of deposition almost coincides with that of dissolution, implying that these two processes are highly reversible when both Pe and $PeDa$ are small.

[41] We also performed simulations with small $PeDa$ and large Pe. The results are not presented in this paper because they are very similar to the previous case. This similarity is
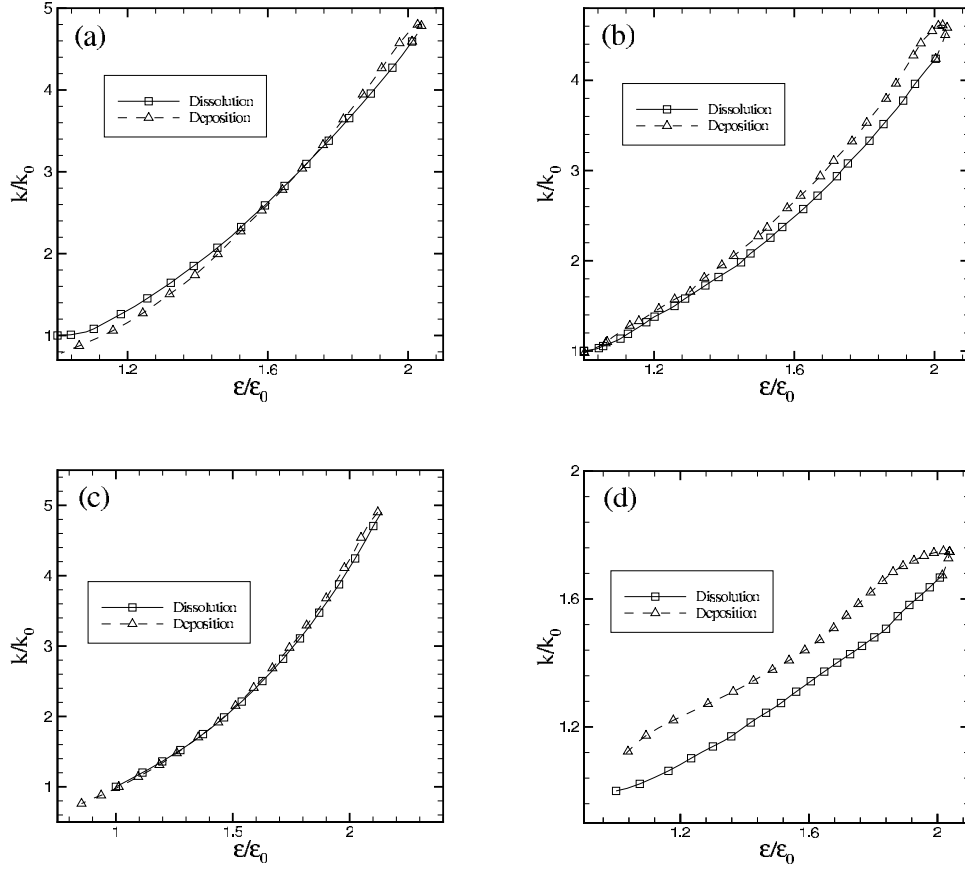
Figure 7. Dependence of permeability on porosity. Both permeability and porosity are normalized by the values of the initial geometry: (a) $Pe = 45$, $PeDa = 7.5$; (b) $Pe = 0.45$, $PeDa = 0.075$; (c) $Pe = 0.0045$, $PeDa = 0.00075$; (d) $Pe = 0.0045$, $PeDa = 7.5$.

in line with *Bekri et al.*'s [1995] conclusion that the effect of the Peclet number is only significant for large *PeDa* values.

4. Conclusions

[42] We have extended an LB model developed previously to study the dissolution/precipitation process in a simplified porous media. We focused on the effects of *Pe* and *PeDa* numbers on the transport and reaction process.

[43] Dissolution principally occurs on the walls that face the inlet boundary and along the walls of the larger fracture if (1) the process is diffusion-limited (*PeDa* > 1) and (2) convection is predominant (*Pe* > 1). Such dissolution results in a wormhole phenomenon in which the initial main flow path becomes even more dominant because of the dissolution.

[44] If (1) the process is diffusion-limited (*PeDa* > 1) and (2) convection is insignificant (*Pe* < 1), dissolution principally occurs on the walls that face the inlet boundary. However, fractures do not grow larger. The system also experiences a slow increase in permeability.

[45] In both cases, precipitation results are similar to those of dissolution, but in the opposite direction. However, the effects of dissolution cannot be reversed by precipitation, even when the reaction driving force has the same magnitude and all other relevant parameters are identical.

[46] If the process is reaction-limited (*PeDa* ≪ 1), dissolution is nearly uniform over all the solid surface. Moreover, precipitation can approximately reverse its effects. In this case, the process is not sensitive to the *Pe* number.

[47] If both *Pe* and *PeDa* are moderate, then the effects of convection, diffusion, and reaction are comparable. The reaction occurs on the walls that face the inlet boundary and on the walls of both fractures; the reaction favors the upstream solid surfaces. The interplay of the various transport mechanisms does not enable dissolution and precipitation to reverse their effects by interchanging with each other.

[48] We selected a simplified medium for this study so that we could conveniently analyze the effects of the control parameters found in the dissolution/precipitation process. However, the conclusions drawn from this study can be readily extended to more realistic porous media because (1) the simplified medium's larger fracture corresponds to the

Table 1. Values of k/k_0 at $\epsilon/\epsilon_0 = 2$ for Different Cases

Case	k/k_0
a	4.59
b	4.23
c	4.21
d	1.67

high permeable regions found in more complex media and (2) the simplified medium's smaller fracture corresponds to the low permeable regions encountered in more complex media. Furthermore, the LB method we used to obtain the results documented in this paper is equally applicable to more realistic porous media, as demonstrated in the single-phase flow study of *Zhang et al.* [2000] and in the dissolution study of *Kang et al.* [2002]. In fact, for the medium used in this study, even though its initial geometry is relatively simple, it becomes quite complex and irregular as a result of dissolution and precipitation.

Notation

|	
C	solute concentration.
C_0	concentration of inflowing fluid.
C_s	saturated concentration.
D	diffusivity.
Da	Damkohler number.
$\mathbf{e}_i$	particle discrete velocity.
f_i	particle distribution function to simulate fluid flow.
f_i^{eq}	equilibrium distribution function of f_i.
g_i	particle distribution function to simulate solute transport.
g_i^{eq}	equilibrium distribution function of g_i.
k_r	reaction rate constant.
L	characteristic length.
p	fluid pressure.
Pe	Peclet number.
$PeDa$	Peclet-Damkohler number.
R	gas constant.
T	temperature.
$\mathbf{u}$	fluid velocity.
ρ	fluid density.
ν	fluid kinematic viscosity.
δ_t	time increment.
τ	relaxation time for f_i.
τ_s	relaxation time for g_i.
ω_i	weight coefficient.

References

Aharonov, E., J. Whitehead, P. B. Kelemen, and M. Spiegelman, Channeling instability of upwelling melt in the mantle, *J. Geophys. Res.*, *100*, 20,433–20,450, 1995.

Aharonov, E., M. Spiegelman, and P. B. Kelemen, Three-dimensional flow and reaction in porous media: Implications for the Earth's mantle and sedimentary basins, *J. Geophys. Res.*, *102*, 14,821–14,833, 1997.

Bekri, S., J. F. Thovert, and P. M. Adler, Dissolution of porous media, *Chem. Eng. Sci.*, *50*, 2765–2791, 1995.

Bekri, S., J. F. Thovert, and P. M. Adler, Dissolution and deposition in fractures, *Eng. Geol.*, *48*, 283–308, 1997.

Chadam, J., D. Hoff, E. Merino, P. Ortoleva, and A. Sen, Reactive infiltration instability, *J. Appl. Math.*, *36*, 207–221, 1986.

Chen, H., S. Chen, and W. H. Matthaeus, Recovery of the Navier-Stokes equations using a lattice-gas Boltzmann method, *Phys. Rev. A*, *45*, R5339–5342, 1992.

Chen, S., and G. D. Doolen, Lattice Boltzmann method for fluid flows, *Annu. Rev. Fluid Mech.*, *30*, 329–364, 1998.

Chen, W., and P. Ortoleva, Reaction front fingering in carbonate-cemented sandstone, *Earth Sci. Rev.*, *29*, 183–198, 1990.

Daccord, G., Chemical dissolution of a porous medium by a reactive fluid, *Phys. Rev. Lett.*, *58*, 479–482, 1987.

Dawson, S. P., S. Chen, and G. D. Doolen, Lattice Boltzmann computations for reaction-diffusion equations, *J. Chem. Phys.*, *98*, 1514–1523, 1993.

Dijk, P., and B. Berkowitz, Precipitation and dissolution of reactive solutes in fracture, *Water Resour. Res.*, *34*, 457–470, 1998.

Fredd, C. N., and H. S. Fogler, Influence of transport and reaction on wormhole formation in porous media, *AIChE J.*, *44*, 1933–1949, 1998.

Hoefner, M. L., and H. S. Fogler, Pore evolution and channel formation during flow and reaction in porous media, *AIChE J.*, *34*, 45–54, 1988.

Janecky, D. R., et al., Lattice gas automata for flow and transport in geochemical systems, in *Proceeding, 7th International Symposium on Water-Rock Interaction*, edited by Y. K. Kharaka and A. S. Maest, pp. 1043–1046, A.A. Balkeema, Brookfield, Vt., 1992.

Kang, Q., D. Zhang, S. Chen, and X. He, Lattice Boltzmann simulation of chemical dissolution in porous media, *Phys. Rev. E*, *65*, 036318, 2002.

Kelemen, P. B., J. A. Whitehead, E. Aharonov, and K. A. Jordahl, Experiments on flow focusing in soluble porous media, with applications to melt extraction from the mantle, *J. Geophys. Res.*, *100*, 475–496, 1995.

Liu, X., A. Ormond, K. Bartko, Y. Li, and P. Ortoleva, Matrix acidizing analysis and design using a geochemical reaction-transport simulator, *J. Pet. Sci. Eng.*, *17*, 181–196, 1997.

Nie, X., G. D. Doolen, and S. Chen, Lattice-Boltzmann simulations of fluid flows in MEMS, *J. Stat. Phys.*, *107*, 279–289, 2002.

Ormond, A., and P. Ortoleva, Numerical modeling of reaction-induced cavities in a porous rock, *J. Geophys. Res.*, *105*, 16,737–16,747, 2000.

Ortoleva, P., J. Chadam, E. Merino, and A. Sen, Geochemical self-organization. II: The reactive-infiltration instability, *Am. J. Sci.*, *287*, 1008–1040, 1987.

Qian, Y., D. d'Humieres, and P. Lallemand, Lattice BGK models for Navier-Stokes equation, *Europhys. Lett.*, *17*, 479–484, 1992.

Salles, J., J. F. Thovert, and P. M. Adler, Deposition in porous media and clogging, *Chem. Eng. Sci.*, *48*, 2839–2858, 1993.

Steefel, C. I., and A. C. Lasaga, Evolution of dissolution patterns: Permeability change due to coupled flow and reaction, in *Chemical Modeling in Aqueous Systems II, ACS Symp. Ser.*, vol. 416, edited by D. C. Melchior, pp. 212–225, Am. Chem. Soc., Washington, D. C., 1990.

Steefel, C. I., and A. C. Lasaga, A coupled model for transport of multiple chemical species and kinetic precipitation/dissolution reactions, *Am. J. Sci.*, *294*, 529–592, 1994.

Wells, J. T., D. R. Janecky, and B. J. Travis, A lattice gas automata model for heterogeneous chemical-reactions at mineral surfaces and in pore networks, *Physica D*, *47*, 115–123, 1991.

Zhang, D., R. Zhang, S. Chen, and W. E. Soll, Pore scale study of flow in porous media: Scale dependency, REV, and statistical REV, *Geophys. Res. Lett.*, *27*, 1195–1198, 2000.

Zou, Q., and X. He, On pressure and velocity boundary conditions for the lattice Boltz-mann BGK model, *Phys. Fluids*, *9*, 1591–1598, 1997.

————————
S. Chen, Department of Mechanical Engineering, Johns Hopkins University, 223 Latrobe Hall, 3400 N. Charles Street, Baltimore, MD 21218, USA. (syc@pegasus.me.jhu.edu)

Q. Kang and D. Zhang, Hydrology, Geochemistry, and Geology Group, Los Alamos National Laboratory, Los Alamos, NM 87545, USA. (qkang@lanl.gov)
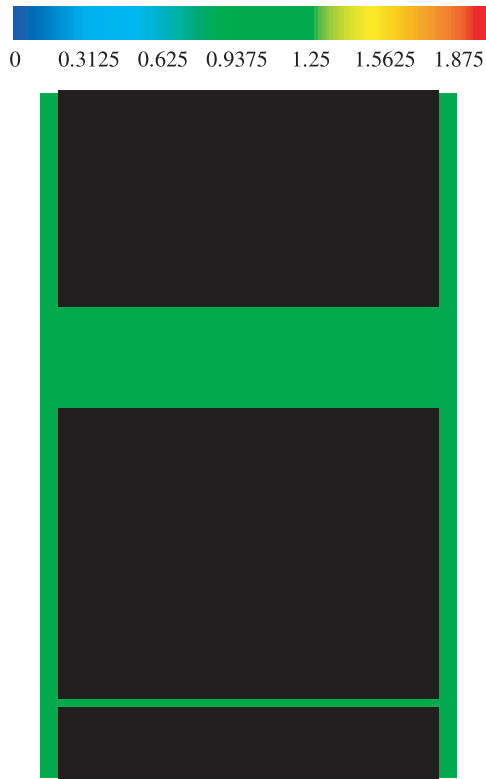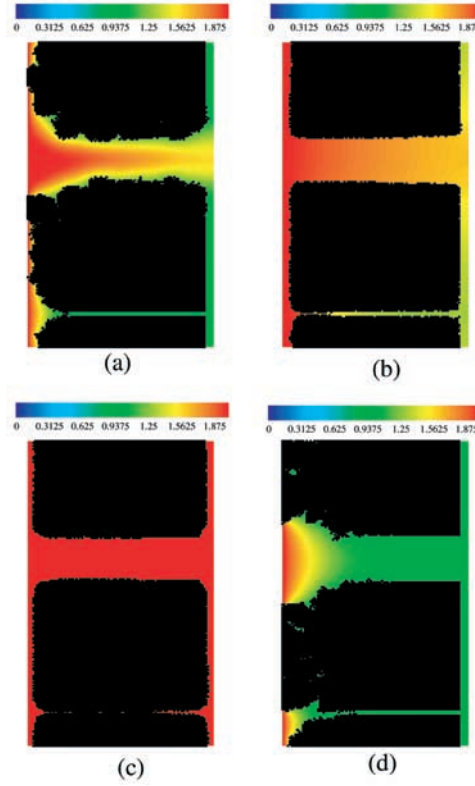
Figure 3. Schematic illustration of the two-dimensional geometry and the initial distribution of the solute concentration.
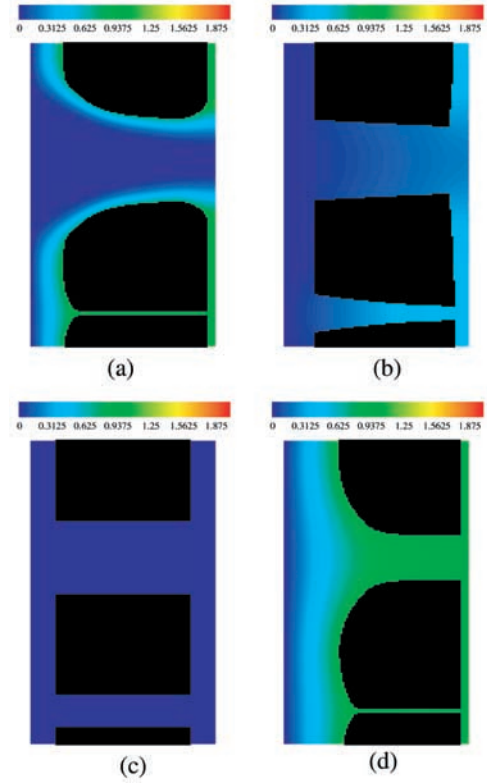
Figure 4. Resulting geometry and distribution of the solute concentration due to dissolution, just before the inflowing fluid is switched from pure solvent to super-saturated solution. The concentration is normalized by the saturated one: (a) $Pe = 45$, $PeDa = 7.5$; (b) $Pe = 0.45$, $PeDa = 0.075$; (c) $Pe = 0.0045$, $PeDa = 0.00075$; (d) $Pe = 0.0045$, $PeDa = 7.5$.

Figure 5. Resulting geometry and distribution of the solute concentration due to precipitation, when a fracture is clogged. The concentration is normalized by the saturated one: (a) $Pe = 45$, $PeDa = 7.5$; (b) $Pe = 0.45$, $PeDa = 0.075$; (c) $Pe = 0.0045$, $PeDa = 0.00075$; (d) $Pe = 0.0045$, $PeDa = 7.5$.